Electronic Supplementary Information

Pd nanoparticles growth monitored by DRIFT spectroscopy of adsorbed CO

Andrei Tereshchenko,*[a] Alexander Guda,*[a] Vladimir Polyakov,[a] Yury Rusalev,[a] Vera Butova[a] and

Alexander Soldatov[a] [a] The Smart Materials Research Institute, Southern Federal University, 344090,

Rostov-on-Don, Russia.

*Corresponding authors: Andrei Tereshchenko, Email: tereshch1@gmail.com; Alexander Guda, Email: guda@sfedu.ru

EXPERIMENTAL SECTION

MATERIALS AND REAGENTS

Cerium (III) nitrate hexahydrate Alfa Aesar 99.5%; palladium (II) chloride Alfa Aesar 99.999%; 5 wt % Pd/Al_2O_3 catalyst (Chimet S.p.A) with a mean size of Pd NPs 2-3 nm (reference sample).

METHODS AND EXPERIMENTAL DETAILS

X-ray fluorescence (XRF) elemental analysis was performed on the Bruker M4 Tornado spectrometer equipped with an XFlash 430 detector in the range from 0 to 26 keV. Signal of fluorescence was collected in more than 20 different points with an acquisition time of 10 s and averaged.

XRF elemental analysis of synthesized samples revealed that real loadings were close to theoretical values (4 wt %): 4.1±0.5 wt% for Pd-150 and 3.9±0.5 wt% Pd-300, and slightly less for Pd-30: 2.6±0.5 wt%.

Density functional theory (DFT) calculations were performed in the Vienna ab initio package (VASP 5.2). [1,2] Projector augmented wave method was chosen to represent the atomic core region in combination with Perdew-Burke-Ernzerhof (PBE) correlation energy functional.[3] The cut-off energy for a plane wave basis set was limited to 600 eV. Calculations were performed for 23 Å cubic box with Pd_{55} cluster in the center (1.1 nm in diameter). Single CO probe molecule was placed on different sites of this nanocluster, forming 7 different structures (Fig. S1). Only gamma point was considered. A conjugate-gradient algorithm was used to relax geometry. IR frequencies were obtained with IBRION 7 flag using a script developed by David Karhanek[4].

X-ray powder diffraction (XRPD) patterns were acquired on the Bruker D2 PHASER diffractometer with Bragg–Brentano geometry using a CuK wavelength (1.5406 Å). Data were collected in the range from 5 to 90° with 0.01° step and 0.4 s acquisition time. Obtained peaks were approximated by the Lorentz function using the Jana2006 code[5].

XRPD didn't allow distinguishing peaks corresponding to both metallic Pd (JCPDS 46-1043) and palladium oxide (JCPDS 41-1107) for all three samples (Fig. S3). Particularly, the most intensive peak related to diffraction on Pd (111) planes was missing. Only a strong signal of ceria support was observed (CeO_2 fluorite structure JCPDS 34-0394). This fact could be explained by the extremely small size of synthesized NPs which caused broadening of peaks and is in a good agreement with results obtained by different authors who reported the difficulties of XRPD analysis of small Pd NPs[6,7]. The mean size of ceria NPs was determined according to the Williamson-Hall approach[8] and it was estimated as 22–24 nm.

Materials were characterized by **transmission electron microscopy (TEM)** using a FEI Tecnai G2 F20 transmission electron microscope (FEI Company, Hillsboro, OR, USA) with an accelerating voltage of 80– 200 kV. TEM image (Fig. S4A) showed the nanocrystalline structure of CeO_2; however, they did not allow us to distinguish Pd NPs from the ceria support straightforwardly due to a low Z-contrast (Z(Pd) = 46 and Z(Ce) = 58). Fourier Transformed image (Fig. S4B) revealed weak diffraction spots related to the diffraction

on Pd (111) planes (red circle with d = 0.22(8) nm) and on PdO (110) and (121) (weak spots on the bigger orange circles, d = 0.21(1) nm and d = 0.13(1) nm). All other spots originated from CeO_2 (green).

DRIFT spectroscopy of adsorbed CO was performed for already synthesized Pd/Al_2O_3 catalyst to obtain spectra of reference material with known particle size at elevated temperatures. Before sending a reducing mixture with CO probe molecules, the Pd/Al_2O_3 sample was heated up to 150 °C in Ar flow (50 ml/min) to remove water and other guest molecules. Then, a mixture of H_2 (2.5 ml/min), CO (1 ml/min), and Ar (46.5 ml/min) was sent to the sample. After 1 hour at 150 °C, the sample was heated to 300 °C in Ar/CO mixture (46.5 and 1 ml/min, respectively), and kept 1 hour at 300 °C. Then the Pd/Al_2O_3 sample was cooled down to the 30 °C. Spectra recorded after stages at 150 and 300 °C were deconvoluted and compared with deconvoluted spectra of Pd-150 and Pd-300 measured at the same conditions (Fig. S5). The scheme of the experiment and obtained spectra are shown in Fig. S6A.

After 10 min at 150 °C in H_2/CO/Ar mixture bridged and linear carbonyls reached their saturation (Fig. S6B). We didn't expect a growth of NPs in the case of already grown reference sample, so all observed changes were attributed to the palladium oxide reduction to metallic state and equilibration processes. Analysis of deconvoluted spectra has shown, that B/L ratios of Pd-150 at 150 °C and Pd-300 at 300 °C sample were less than observed for Pd/Al_2O_3 at the same temperatures (Table S2). It means that the size of NPs in the case of Pd-150 and Pd-300 samples was less than the size of the reference sample. That fact is in good agreement with results obtained at room temperature (see Table 3 in the main text) and it was confirmed that such estimation could be performed at elevated temperatures.

Tests of catalytic activity in CO oxidation reaction were performed in the home-made catalytic chamber (Fig. S7). 30 mg of powdered sample was placed between two pieces of cotton in the chamber. For Pd-150, Pd-300, and Pd/Al_2O_3 reference samples reducing pretreatment in the mixture of H_2 (2.5 ml/min) and Ar (47.5 ml/min) at 120 °C for 1 h was performed. For Pd-30 oxidizing pretreatment was done in the flow of O_2 (10 ml/min) and Ar (40 ml/min) at 200 °C for 1h. After this sample was cooled down to the 30 °C in the flow of Ar (47.5 ml/min). Then reaction mixture of CO (1 ml/min), O_2 (4.5 ml/min), and Ar (47.5 ml/min) was sent through the catalytic chamber with the sample. The material was heated to 215 °C in conditions of oxygen excess (O_2/CO molar ratio was 4.5). Gas outlet of the chamber was connected with a gas cell (High Temperature Cell, Harrick Scientific Products Inc, New York, USA) installed Vertex 70 spectrometer and used to measure infrared spectra in the transmission geometry of gas products after reaction mixture passing the sample. Before sending the reaction mixture through the sample it was sent through the bypass to the gas cell for recording a spectrum of CO at zero conversion for further normalization. FTIR spectra of exhaust gases from the catalytic chamber were recorded at fixed temperatures and steady-state conditions. The areas under peaks attributed to CO and CO_2 peaks (ca. 2143 and 2330 cm^{-1}, respectively) were recalculated to the percent of CO conversion and, further, to the amount of CO converted per time and mass of Pd.

According to the results of catalytic activity tests, all samples were less active than Pd/Al_2O_3 reference sample and didn't reach 100% of conversion below 215 °C (Fig. S8). After recalculating on Pd loading, it was observed that Pd-300 was less active then Pd-150. Pd-30 demonstrated higher activity at low temperature (below
~130 °C) whereas at higher temperature activity become close to one's of Pd-150 and Pd-300 samples. Higher activity at low temperature was caused probably by the pretreatment in an oxidizing atmosphere in the case of Pd-30 unlike reduction performed for all other samples.

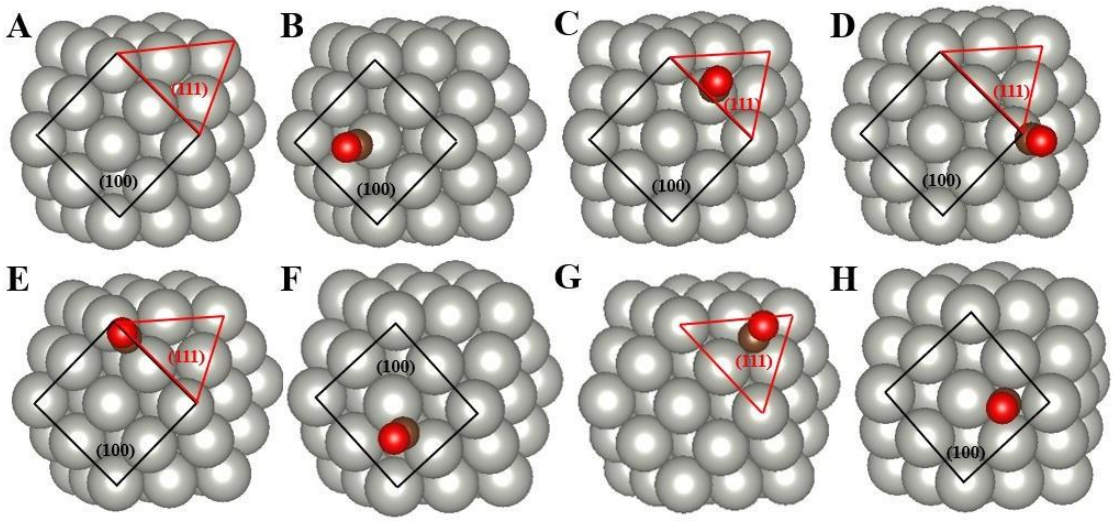

Fig. S1 Relaxed structure of (A) Pd_{55} cluster. CO molecules atop adsorbed on (B) Pd(100) facet, (C) particle edge and (D) corner (linear carbonyls), CO adsorbed on 2-fold sites of (E) particle edge and (F) Pd(100) facet; (G) 3-fold Pd(111) facet and (H) 4-fold Pd(111) facet (bridged carbonyls).

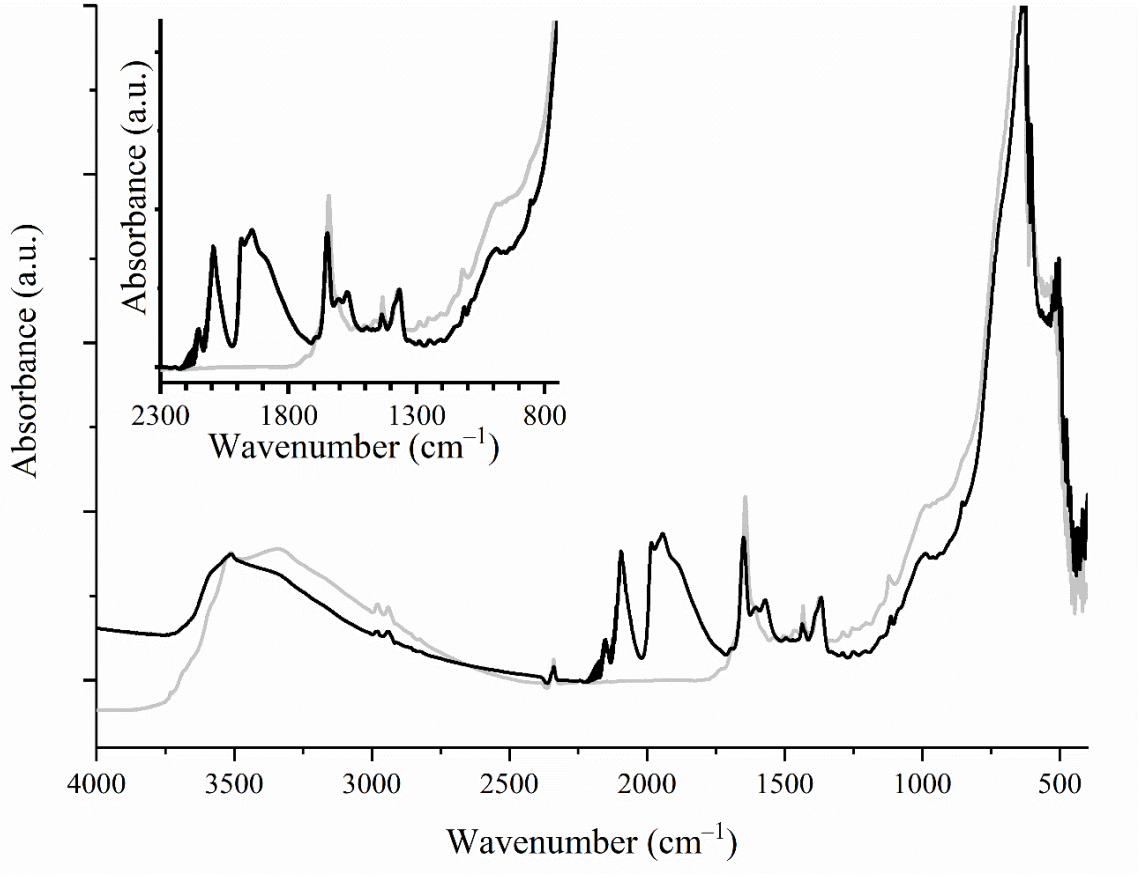

Fig. S2. DRIFT spectra during the synthesis of Pd-30 sample before (grey) and after reduction (black) of $PdCl_2/CeO_2$ in H_2/CO mixture.

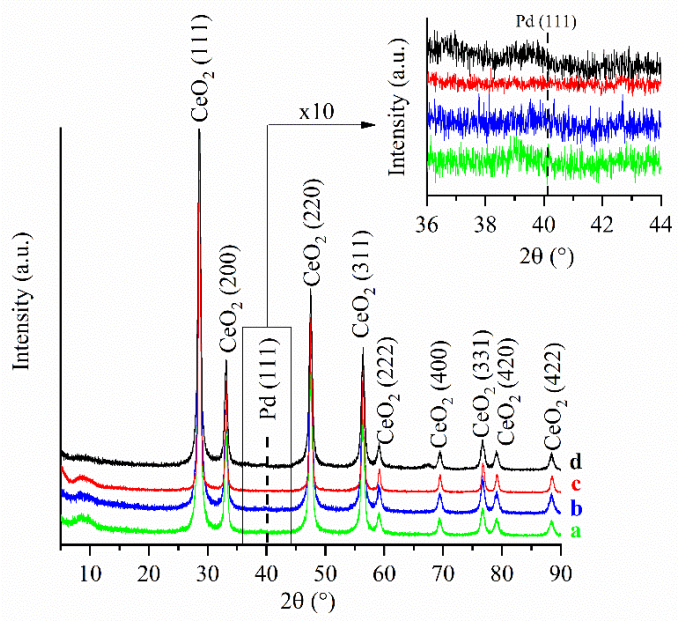

Fig. S3 XRPD patterns of Pd-300 (a), Pd-150 (b) and Pd-30 (c) and CeO_2 support (d). λ(CuKα) = 0.15406 nm. Peaks related to diffraction on Pd are
not visible (the magnified region where the most intensive diffraction peak of Pd(111) should be located is shown in the inset).

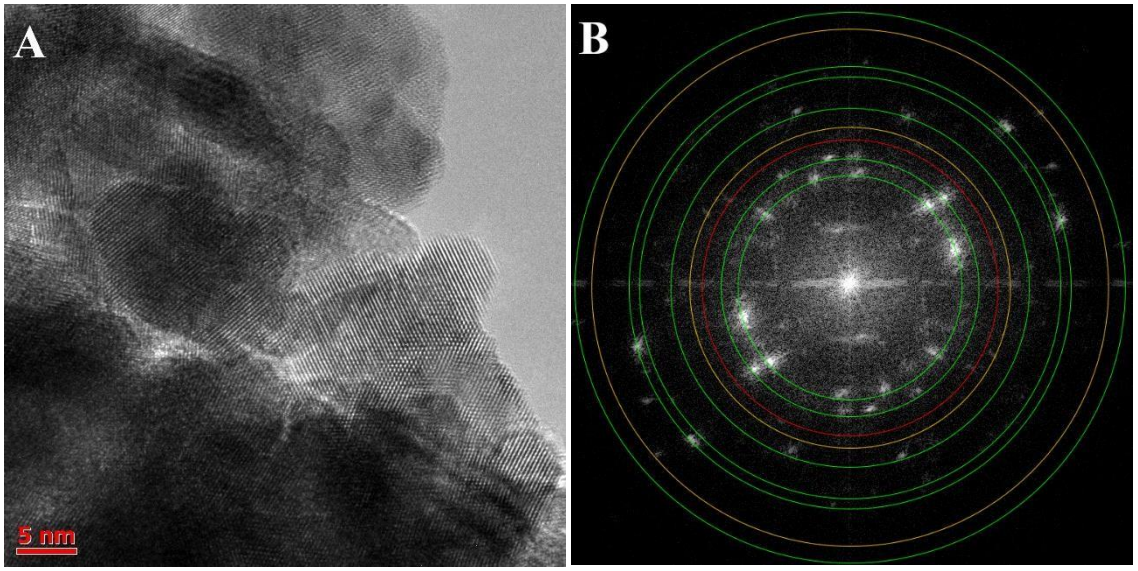

Fig. S4 (A) TEM micro-image of Pd-300 and (B) Fourier Transformed Image with circles related to diffraction on Pd (red), PdO (orange), and CeO_2 (green).

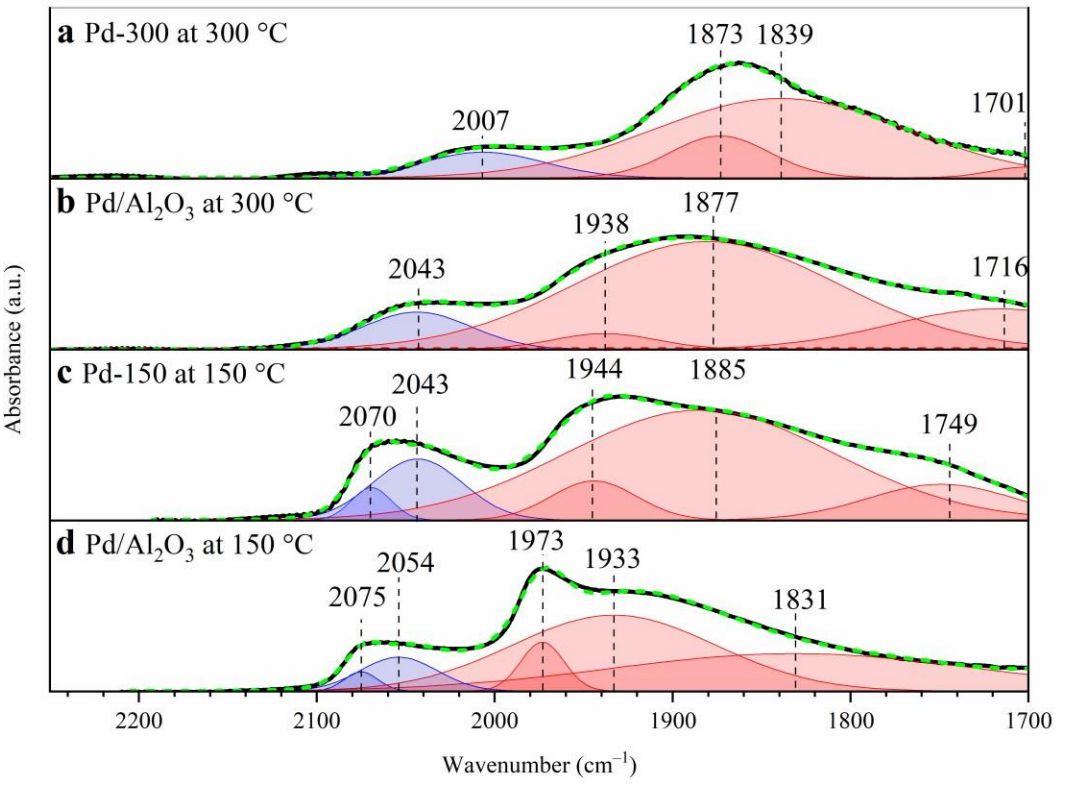

Fig. S5 Deconvolution of in situ FTIR spectra after reduction at 300 °C of Pd-300 (a) and Pd/Al_2O_3 reference sample (b), after reduction at 150 °C of Pd-150 (c) and Pd/Al_2O_3 reference sample (d). All spectra are shown after subtracting the CO gas phase component. Analysed FTIR spectra are black, Gaussian functions used for approximation blue for linear and red for bridged carbonyls. Cumulative fit peaks are shown by the dashed green line.

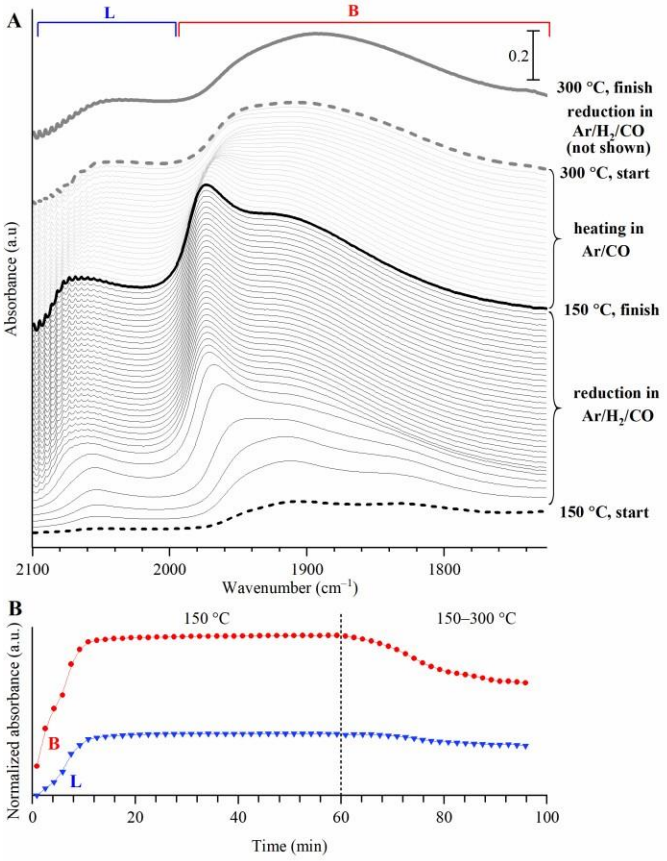

.

Fig. S6 (A) A series of FTIR spectra in $CO/H_2/Ar$ or CO/Ar gas mixtures sent to commercial catalyst Pd/Al_2O_3. Spectra were acquired every 100 seconds. Spectra before and after reduction at 150 °C are dashed and bold black, respectively. Spectra during heating at 150 °C are
thin black. A series of spectra during heating from 150 to 300 °C is grey. Spectra before and after reduction at 300 °C are dashed and bold solid gray, respectively (intermediate spectra at 300 °C are not shown). Curve for 300 °C was shifted vertically for clarity (B) Changes
of absorbance in peak amplitudes in the regions of linear (blue) and bridged carbonyls (red) during the reduction of Pd/Al_2O_3.

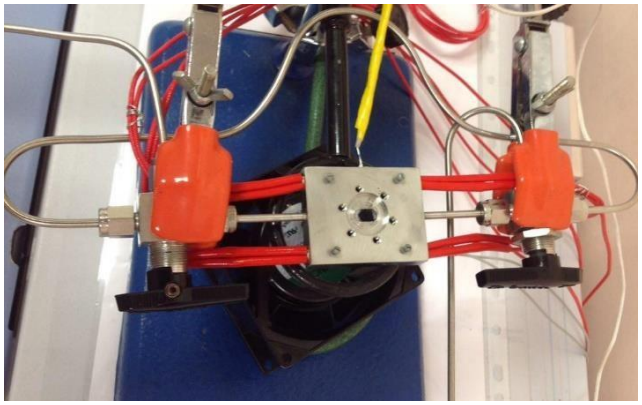

Fig. S7 Catalytic chamber with catalyst inside placed between two pieces of quartz wool.

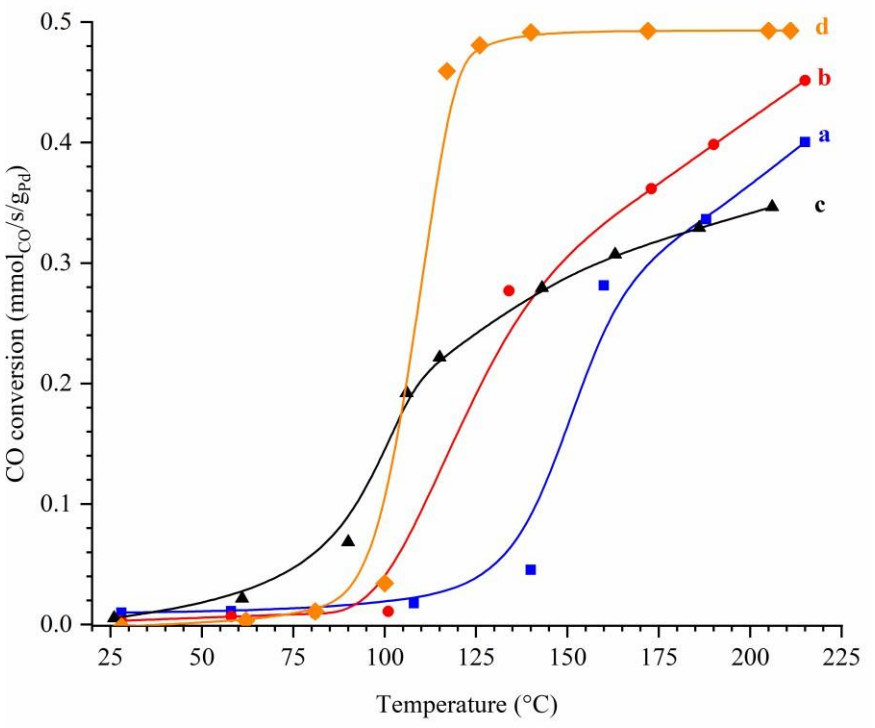

Fig. S8 CO conversion recalculated to mmol/s/g_{Pd} vs oxidation reaction temperature in a mixture of 1.9% CO, 8.5% O_2 and 89.6% Ar at a total flow rate of 53 mL/min[1] for Pd-300 (a), Pd-150 (b), Pd-30 (c) and Pd/Al_2O_3 reference sample (d). The molar ratio of O_2/CO = 4.5.

Table S1. Peak positions and normalized areas under the peaks of carbonyls at 30 °C.

Sample	Time since the start of reduction, min	ν, cm^{-1} /Area, %								B/L area ratio
		CO adsorbed on ions		Linear carbonyls (L)		Bridged carbonyls (B)				
		Pd^{2+}	Pd^{+}	a-top on well dispersed but non-crystalline Pd	a-top on defects (edges, steps, etc)	2-fold on Pd(100) / defects	2-fold on Pd(111)	3-fold on Pd(111)	4-fold or metal-support interface	
Pd-30	15	2149.9	2111.5	2099.4	2084.1	1972.6	1936.4	1884.9	1753.8	1.48
		6	3.2	9.7	27	4.6	7	40.2	2.4	
	20	2150.4	2113.5	2097.1	2088.2	1979.3	1946.7	1892.1	1763.5	2.03
		4.6	1.7	5.1	25.8	3.6	9.6	44.7	4.8	
	25	2150.6	2114	2095.8	2087.5	1981.8	1952.2	1896.1	1781	2.39
		4	1.2	4.4	23.6	3.3	12.2	42.7	8.6	
	40	2150.3	2114.6	2094.5	2083.8	1984.3	1957.3	1904.3	1803.8	3.12
		3	0.6	3.9	19.5	3.4	13.9	40.4	15.4	
	60	2149.7	2114.6	2094.1	2080.1	1985.3	1959.3	1910.6	1816.2	3.76
		2.1	0.2	4	16.5	3.6	13.4	39.3	20.8	
Pd-150	60	2139.2	—	2086.8	2059.3	—	1948.4	1907.4	1784.2	3.2
		0.4		6.6	17.1		6.4	47.1	22.4	
Pd-300	60	2129.9	—	2076	2051.4	—	1952.8	1909.2	1798.8	2.33
		1.8		6.6	22.9		3.7	60.0	5.0	
Pd/Al_2O_3	60	2138.3	—	2087.9	2066.4	1980.4	1953.7	1922.9	1797.7	5.5
		0.3		2.5	8.1	3.3	4.4	26.2	24.4	

Table S2. Peak positions and normalized areas under the peaks of carbonyls after the reduction at elevated temperatures.

Temperature, °C	Sample	ν, cm^{-1} /Area, %						B/L area ratio
		Linear carbonyls (L)		Bridged carbonyls (B)				
		a-top on well dispersed but non-crystalline Pd	a-top on defects (edges, steps, etc)	2-fold on Pd(100) / defects	2-fold on Pd(111)	3-fold on Pd(111)	4-fold or metal-support interface	
300	Pd-300	—	2006.6	—	1873.4	1839.4	1700.7	8.1
			11		14.7	71.5	2.8	
	Pd/Al_2O_3	—	2043.8	1938.3	1880.8	—	1717.7	9.5
			9.5	3.8	66.3		20.4	
150	Pd-150	2069.4	2043.4	1944.3	1884.6	—	1748.9	5.6
		2.9	12.3	7.5	66		11.3	
	Pd/Al_2O_3	2075.2	2054	1973.3	1933	1831.6	—	9.6
		1.9	7.6	6.2	44.7	39.7		

References

1. G. Kresse and J. Furthmüller, *Phys. Rev. B*, 1996, **54**, 11169.
2. G. Kresse and J. Furthmüller, *Comput. Mater. Sci.*, 1996, **6**, 15-50.
3. J. P. Perdew, K. Burke and M. Ernzerhof, *Phys. Rev. Lett.*, 1996, **77**, 3865.
4. D. Karhanek, Github: VASP infrared intensities, https://github.com/dakarhanek/VASP-infrared-intensities, (accessed June, 2020).
5. V. Petříček, M. Dušek and L. Palatinus, *Z. Kristallogr. Cryst. Mater*, 2014, **229**, 345-352.
6. A. Baylet, P. Marécot, D. Duprez, P. Castellazzi, G. Groppi and P. Forzatti, *Phys. Chem. Chem. Phys.*, 2011, **13**, 4607-4613. 7. W. Zhou and J. Y. Lee, *J. Phys. Chem. C*, 2008, **112**, 3789-3793.
8. G. Williamson and W. Hall, *Acta Metall.*, 1953, **1**, 22-31.